ISSN 0031-918X, Physics of Metals and Metallography, 2021, Vol. 122, No. 13, pp. 1257–1263. © Pleiades Publishing, Ltd., 2021.
ISSN 0031-918X, Physics of Metals and Metallography, 2021. © Pleiades Publishing, Ltd., 2021.

THEORY OF METALS

First-Principles Study of Mechanical and Electronic Properties of η and η' Phases Present in 7xxx Alloys

Yunlong Ma[a, b, *], Ben Lin[c], Zhengbing Xiao[d], and Yuanchun Huang[d]

[a] *Institute of Advanced Structure Technology, Beijing Institute of Technology, Beijing, 100081 China*
[b] *Beijing Institute of Astronautical Systems Engineering, Beijing, 100076 China*
[c] *China Academy of Launch Vehicle Technology, Beijing, 100076 China*
[d] *Central South University, Changsha, 410000 China*
**e-mail: mayunlong@bit.edu.cn*

Received March 4, 2020; revised July 15, 2020; accepted July 21, 2020

Abstract—The η' and η strengthening precipitates in Al–Zn–Mg alloys were investigated by the first principle calculations. Results of the heat of formation and cohesive energy indicates that the model of η' with $P\overline{6}$ and space group of No. 174 is the energy favored model. The structure, elastic constants and electronic properties of the energy favored η' and η ($MgZn_2$) were compared and discussed. The obtained negative heat of formation and cohesive energy indicates that both η' and $MgZn_2$ have good alloying ability and structural stability, while $MgZn_2$ particles exhibit a higher structural stability compared to η', for $MgZn_2$ has a lower density of states (DOS) at the Fermi level, which was verified by the experiments that η' is not as stable as $MgZn_2$. In addition, the obtained elastic constants C_{ij} of $MgZn_2$ and η' were calculated, from which were derived the elastic modulus such as bulk modulus (B), shear modulus (G), Poisson ration (ν), Young's modulus (E), and anisotropy (A) of these two precipitates. It is suggested that $MgZn_2$ is stronger than η' for the higher elastic constants but with a better isotropy. Finally, the electronic density of states of η' and $MgZn_2$, together with their influences to the mechanical performance of Al–Zn–Mg alloys were furtherly discussed.

Keywords: Al–Zn–Mg alloys, first-principles, elastic properties, precipitates

DOI: 10.1134/S0031918X20140112

1. INTRODUCTION

Al–Zn–Mg based aluminum alloys have been widely investigated and used for the transportation applications, both for the cars, trains and the airplanes, due to the light weight and high strength, which are governed by the precipitates presented in the alloy greatly [1–4]. This kind of alloys with zinc and magnesium as major alloying elements, precipitation strengthening can be obtained by heat treatment. Of all the precipitates, the metastable phase η' and stable phase η play the most important role in controlling the mechanical performance of the alloy, considerable investigations revealed that η' and η are responsible for the hardening effect in the peak-aged heat treatment and over-aged heat treatment, respectively [5, 6]. The η' phase is regarded as the prim-precipitate of the equilibrium η phase, it is generally present in those alloys aged to peak strength. While for the equilibrium phase η, it is found most in the alloys of over-aged state, after the over-aged heat treatment, a better corrosion resistance is obtained but at the cost of strength for the alloy (e.g. T74 temper as compared to T6 peak-aged temper) [2, 3, 5]. Strengthening of the alloy is usually controlled by the kinds of precipitates, which in turn is determined by the strain and interfacial energies of the precipitates to the matrix system, while those properties are sensitive to the crystal structure of matrix phase and relationships between them [7]. As a metastable phase, η' has been widely studied both in composition and structure. At first, an orthorhombic structure with stoichiometry $MgZn_2$ has been proposed by Gjonnes and Simensen for η' [8], but later criticized by Auld and Cousland by XRD using the single crystals, and concluded η' is a hexagonal model with the approximate composition of $Mg_4Zn_{11}Al$ [9]. However, a collection of X-ray intensities performed by Regnier, P.C. indicated poor fit to the model of $Mg_4Zn_{11}Al$, and obvious discrepancies were found between two diffraction data sets [10]. In 2001, based on the model of Auld and Cousland, C. Ravi proposed a model with a composition of $Mg_4Zn_{13}Al_2$ from a view point of total energy calculation, but this model was not confirmed by any experiment observations until now [11]. Then, by high resolution transmission electron microscopy (HRTEM), Li et.al confirmed that η' phase is of hexagonal lattice with space group $P\overline{6}$ and with the composition of $Mg_2Zn_{(5-x)}Al_{(2+x)}$ [12]. Using Patterson analysis and intensity comparisons,

A. Kverneland et al. furtherly proposed another structure model for η' phase, which belongs to the space group of P63/mmc [13]. After years of hot debate about the structure of η', it is generally accepted by most researchers that η' has a hexagonal structure, and its lattice parameters are as follow, a = 4.096 Å, and c = 14.02 Å, [7, 9, 12, 13], the models proposed by Li et al. [12] and A. Kverneland et al. [13] are believed to be the structure of η' and accepted most by other researchers on the basis of their experiments [14–20].

The η phase is a stable phase of hexagonal structure, its space group is $P63/mmc$, each unite cell contains 12 atoms, incoherent with the α-Al [8, 21], and its chemical composition is $MgZn_2$. Several structural and theoretical studies of the η phase have been reported [22, 23], but systematic study on the structural stability, electronic and elastic properties of η is scare, especially in comparison with η', while this information is vital in understanding the age-hardening phenomenon. Transformation of metastable η' to stable phase η is complicated, further investigation is needed. Obviously, precise determination of such phases by experiments, especially the metastable phases is quite difficult. Fortunately, first-principles calculations demonstrated its high reliability in studying their phase transformation and properties [24, 25].

In the present work, the total energy for the models of η' proposed by Li et al. [12] and A. Kverneland [13] is calculated using the first-principles, then the elastic constants and electronic structure of the energy favored model (judged from the value of the heat of formation energy) are furtherly investigated, and comparison between the stable phase η was also made, which would provide valuable data for better understanding, optimization, designation and heat treatment of Al–Zn–Mg alloys, by controlling the vital phases which enhancing the mechanical performance a lot.

2. FIRST-PRINCIPLES METHODOLOGY

The density functional theory (DFT) [26] calculations were performed using the Cambridge sequential total energy package (CASTEP), and ultrasoft pseudopotential [27] was used. Because the DFT with standard local density approximation (LDA) [28, 29] is insufficient in describing the properties of the 3d transition metals, but generalized gradient approximation (GGA) [30] can largely remove the error, so the Perdew–Burke–Ernzerhof (PBE) version of the GGA (GGA–PBE) was adopted for the exchange–correction functional. All calculations were fully relaxed including cell vectors, volume and the internal atomic positions. The cutoff energy of 450 eV for η, 400 eV for Li et al.'s model [12] and 380 eV for A. Kverneland et al. model [13] were found enough to get sufficient convergence respectively, the K-point configuration of 12 × 12 × 12, 9 × 9 × 6 and 8 × 8 × 6 centered at Gama point were used, respectively. The convergence criterion for the calculation were set as below, 5×10^{-6} eV/atom was used as the energy tolerances for geometry optimization, the stress within 0.02 GPa, while 0.01 eV/Å, was applied as the maximum ionic Hellmann–Feynman force, and the ionic displacement is smaller than 5×10^{-4} Å. All the DFT calculations were performed at 0 K, and the equivalent hydrostatic pressure was spplied. Since the method of Voigt could provide the maximum limits of the polycrystalline elastic modulus, while minimum for Reuss, so both modulus calculations of η and η' were performed using Reuss and Voigt methods [31], and the arithmetic averages of Vogit and Reuss value were used here for the investigation.

3. RESULTS AND DISCUSSION

3.1. Investigation of Crystal Structure and Stability

Both η and η' phase have hexagonal structure, but η phase with space group P63/mmc (no. 194), and 12 atoms contained in the unit cell [21], η' model of Li et al. of space group $P\bar{6}$ (no. 174) and containing 22 atoms per unit cell [12], while with space group $P63/mmc$ and 18 atoms per unite cell for the model proposed by A. Kverneland et al. [13]. Experimental data were used as initial input for geometry optimization. Figure 1 shows the fully optimized (using GGA) structure of η and the models of η' phase.

The heat of formation (H) is defined as the energy change during the formation of a crystal from atoms. A negative value indicates an exothermic process and a spontaneous reaction, and lower value implies an easier process of formation, and a more stable phase. While a positive value reflects the formation of the precipitate needs extra heat to promote, and the phase formed is not so stable. The cohesive energy (E) is referenced as the energy needed when the phase decomposes into single atoms, usually, lower cohesive energy means higher structural stability. The value of states at Fermi level (E_F) can denote the stability of the phase, the lower the value, the more stable the phase will become [32].

Throughout the investigation, the heat of formation (H), cohesive energy (E) and value of states at Fermi level (nE_F) were used to judge of stability of the precipitates. The equations to calculate the H and E for a typical binary phase A_xB_y are shown below [33, 34],

$$H = \frac{1}{x+y}\left(E_{tot} - xE^A_{solid} - yE^B_{solid}\right), \quad (1)$$

$$E = \frac{1}{x+y}\left(E_{tot} - xE^A_{atom} - yE^B_{atom}\right). \quad (2)$$

Where E_{tot} is the total energy of the relaxed unit cell, E^A_{solid} and E^B_{solid} are the energies of the constituents A and B, each in the equilibrium (zero-pressure)

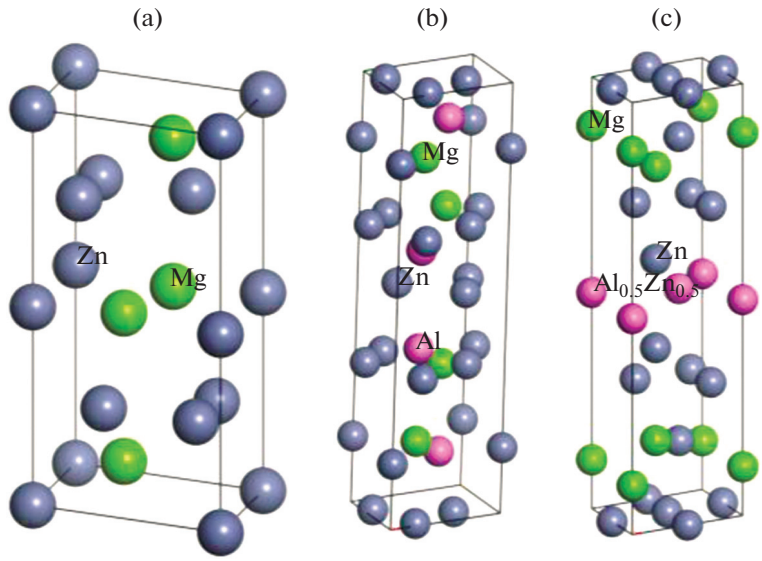

Fig. 1. The crystal structure of η (a), Li et al. model (b), A. Kverneland et al.'s model (c).

geometry. E^{A}_{atom} and E^{B}_{astom} are the total energies of the isolated atoms of A and B in the free state, and x, y are the number of atoms for A and B in the unit cell. Value of states at Fermi level can be got from the DOS calculation.

The obtained lattice parameters, heat of formation, cohesive energy and value of states at Fermi level of η and two η' models are listed in Table 1, so do those of pure aluminum as a reference. The fairly good agreement between experimental and theoretical results for the lattice parameters shows the reasonable calculation parameters of the present calculation. The negative values for heat of formation and cohesive energies of η indicates an exothermic reaction, which correspond to experiments that η is a stable phase. While for the models of η', it could be deduced that heat of formation for the A. Kverneland et al. model [13] is positive, up to 280.3619 eV/atom, which means the model is not an energy favored and is impossibly existent in the viewpoint of energy, at least extra energy for its formation process is needed. Comparatively, the Li et al. model has a lower heat of formation below zero, which implies that the formation of this model is a spontaneous reaction, and it can exist stably. What's more, according to the cohesive energy and value of states at Fermi level, the Li et al. model is more stable than the A.Kverneland et al's. In addition, it can't be neglected that both heat of formation and cohesive energy of η are lower than that of the Li et al.'s model. Hence, η behaves higher structural stability than Li et al. model—a metastable phase, approved by experiment results [35]. To investigate the effects of η and η' to the mechanical properties of the aluminum matrix, the energy favored η' model proposed by LI et.al (here after, LI model is labeled as η') is used for further study.

3.2. Elastic Properties

Elastic constants are the indicators for the response of the crystal to external stresses, they are highly correlated with the possibility of materials failure, those constants are important in understanding the mechanical behaviors of the materials. The elastic constants were calculated using the stress–strain

Table 1. The calculated and experiment lattice constants (a, b, and c, in, Å), volumes of unit cell V_0 (in, Å^3/cell), as well as heat of formation H, eV/atom and cohesive energy E, eV/atom for η and η' phases

Phase			Lattice constants, Å $a = b$, c	c/a	V_0	H, eV/atom	E, eV/atom	E_F, states/eV/atom
η	Li et al.	Calculated	5.21283, 8.49647	1.6299	199.948	−0.2026	−1.3960	4.041
		[8]	5.2234, 8.5562	1.6381	202.171	−0.1428 [22]	−1.3767 [22]	–
η'	A. Kverneland et al.	Calculated	5.0063, 14.0544	2.8073	305.061	−0.0177	−1.623	7.186
		[12]	4.96, 14.02	2.8266	298.075	–	–	–
		Calculated	5.0217, 14.5792	2.9032	318.397	280.3619	242.814	35.09
		[13]	4.96, 14.02	2.8266	198.075	–	–	–

Table 2. The calculated experimental elastic constants C_{ij} (GPa) for η and η'

Phases		C_{11}	C_{33}	C_{44}	C_{12}	C_{13}
η	Calculated	89.16	139.22	20.76	83.49	21.41
	[23]	85.84	133.35	19.81	84.17	19.86
η'	Calculated	99.94	67.94	5.45	57.50	23.09

approach, by the further analysis of the variations in the total energy corresponding to the applied strains to the equilibrium unit cell. A linear relationship between stress (σ) and strain (ε) can be obtained according to the Hook's law, and the relationship between the elastic constant C_{ij} and stress (σ) can be written as,

$$\sigma_i = \sum_{j=1}^{6} C_{ij}\varepsilon_{ij}. \tag{3}$$

The bulk modulus (B), shear modulus (G), Poisson's ration (ν), and young's modulus(E) of η and η' were calculated after the geometry optimization.

For phases with hexagonal structure, there are five independent elastic constants (C_{11}, C_{33}, C_{44}, C_{12} and C_{13}), carried out by the method introduced above. The mechanical parameters got from CASTEP calculations are shown in Table 2.

For the phases of hexagonal, the elastic constants must obey the following rule to guarantee the mechanical stability [23]

$$\begin{gathered} C_{11} > 0,\quad C_{11} - C_{12} > 0,\quad C_{44} > 0, \\ (C_{11} + C_{12})C_{33} - 2C_{13}^2 > 0. \end{gathered} \tag{4}$$

Obviously, results calculated by Castep obey quite well the equation (4), which means the mechanical stability of the phase η and η'. The polycrystalline elastic modulus were estimated using the Voigt–Reuss–Hill (VRH) approximation based on the independent single-crystal elastic constants bove, which can be expressed as Eqs. (5)–(8) [36]

$$B_V = (1/9)[2(C_{11} + C_{12}) + 4C_{13} + C_{33}], \tag{5}$$

$$B_R = \left[(C_{11}+C_{12})C_{33} - 2C_{13}^2\right] \Big/ (C_{11}+C_{12}+2C_{33}-4C_{13}), \tag{6}$$

$$\begin{gathered} G_V = (1/30) \\ \times [C_{11} + C_{12} + 2C_{33} - 4C_{13} + 12(C_{44} + C_{66})], \end{gathered} \tag{7}$$

$$\begin{gathered} G_R = (5/2)\left[(C_{11} + C_{12})C_{33} - 2C_{13}^2\right] \\ \times C_{44}C_{66} \Big/ \{3B_V C_{44}C_{66} \\ + \left[(C_{11} + C_{12})C_{33} - 2C_{13}^2\right](C_{44} + C_{66})\}. \end{gathered} \tag{8}$$

Finally, the VRH mean values can be expressed as Eqs. (9), (10)

$$B = \frac{1}{2}(B_V + B_R), \tag{9}$$

$$G = \frac{1}{2}(G_V + G_R). \tag{10}$$

The Poisson ration can be calculated using the equation as follow:

$$v = (3B - 2G)/2(3B + G). \tag{11}$$

While E was calculated by the G and B, and the formula is shown below [36, 37],

$$E = 9BG/(3B + G). \tag{12}$$

And the formula to calculate the index of anisotropic is as follows

$$A = \frac{(2 * C_{44} + C_{12})}{C_{11}}. \tag{13}$$

The calculated results are presented in Table 3. B is an indicator of the resistance to the volume change by applied pressure [38], bigger B value means the material has stronger resistance to the pressure. So the larger B of η shows its resistance to volume change surpasses that of η'. G measures the resistance to revisable deformations upon shear stress, and the larger value means more directional bonding between atoms. While the E is considered as the measurement of the stiffness of the phases, definitely, the bigger the Young's modulus is, the stiffer the precipitate is. The present calculated results indicate that Al has the largest shear modulus and Young's modulus, and then followed by η and η'. It could be drawn that directional bonding in Al is much stronger than η, not to mention η'. So, it is concluded that it is the coherency between η' and α-Al responsible for the peak-aging (T6) phenomenon, rather the nature of η'. The elastic anisotropy of compounds play a important role in engineering science, and it is highly correlated with the possibility of inducing micro-cracks in materials [40, 41]. So, the index of anisotropic (A).

is usually used as an indication of the anisotropic properties of the phases. In the present work, the value is 1.40 for η and 1.74 for η' respectively, indicating that η' is essentially anisotropy and η is bit anisotropy.

3.3. Electronic Structure

To unveil the nature of bonding interactions within the two precipitates, the total and partial DOS of the constituent Al, Mg and Zn for the η and η' precipitates were calculated and plotted and shown in Fig. 2. The

Table 3. The calculated bulk modulus (B, GPa), shear modulus (G, GPa), Young's modulus (E, GPa), Poisson's ration (ν) and anisotropy factor (A) for polycrystalline η ($MgZn_2$) and η' ($Mg_2Zn_{(5-x)}Al_{(2+x)}$)

Phase	B_V	B_R	B_{VRH}	G_V	G_R	G_{VRH}	E	ν	A
Al*	81.97	81.97	81.97	28.84	28.61	28.73	76.88	0.34	1.09
η	63.35	63.26	63.31	27.14	21.46	24.30	64.63	0.33	1.40
η'	52.80	47.92	50.36	17.37	10.12	13.74	37.78	0.37	1.74

* Calculated from [39].

x-axis is the energy relative to the Fermi level (E_F), Fermi level (E_F) is set to "0" and used as a reference here. Both Fig. 2a for η and Fig. 2b for η' indicate the precipitates exhibit metallic character since the DOS at Fermi energy is non–zero, and the bonding interactions are mainly occupied by the valence electrons of Mg and Zn atoms.

For η phase shown in Fig. 2a, it can be seen that the calculated total DOS is mainly occupied by Mg(p) states and Zn(p), Zn(s) states. The hybridization between valence electrons of Mg and Zn is clear in the entire region, and the variation of hybridization is small. Further, there are two so-called quasigaps near the Fermi level. Usually, a quasigap near the Fermi level implies the directional covalent bonding, the phase with this characteristic indicates a higher strength of the material in comparison with the pure metallic bonding, and the quasigap near the E_F in the bonding region suggests the system has a pronounced stability [22].

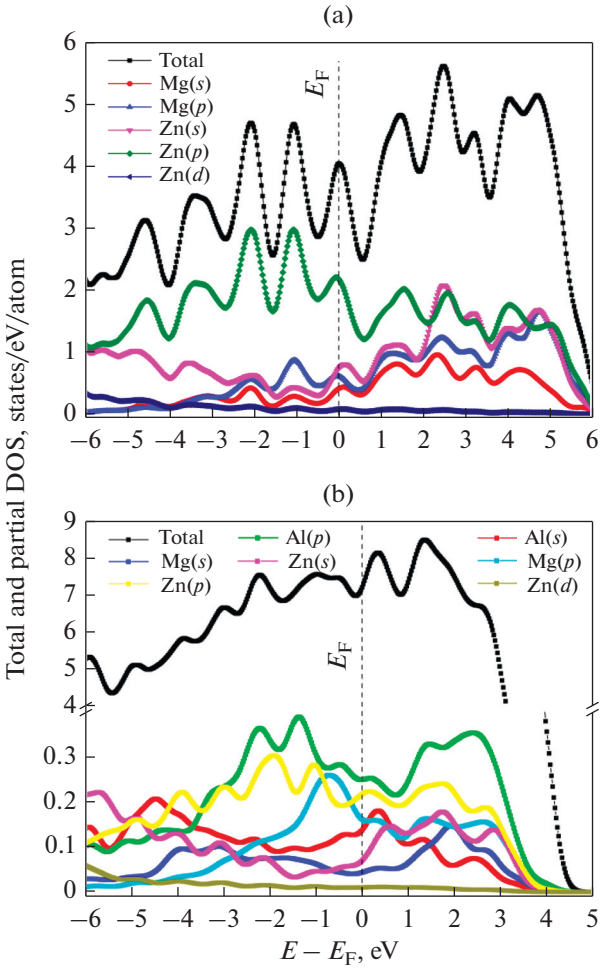

Fig. 2. The total and partial density of states (DOS) of η (a) and η' proposed by Li et al. (b), the Fermi level is set at zero energy and marked by the vertical lines.

While for η' phase as show in Fig. 2b, the energy region and contribution of the valence electrons are different from that of η phase for the participation of Al element. The bonding peak for η' precipitate is predominantly derived from the valence electrons of Al(p), Zn(p) and Mg(p) orbital. Also, there is a quasigap near Fermi level, meaning the covalent bonding for η' just like η, but the DOS at Fermi level for η' is found higher than that of η. Usually, the smaller the (nE_F) indicates the more stable the compound will becomes [32]. Based on the calculated heat of formation H presented in Table 1 and the electronic structure results, η is more stablethan η' phase, which is in good accordance with the experiment phenomenon [42].

4. CONCLUSIONS

In this paper, the heat of formation, cohesive energy of the stable phase η and two models proposed of metastable phase η' were investigated by ultrasoft pseudopontentials based on DFT within the GGA. The η' model suggested by Li et al. of hexagonal structure ($P\overline{6}$, no. 174) is the energy favored model, for its lower heat of formation, cohesive energy and value of state at Fermi level compared to another model with space group $P63/mmc$. The crystal structural properties, elastic constants including the bulk modulus, shear modulus, Young's modulus, Poisson's ration, anisotropy factor and electronic properties of η and Li's model for η' have been investigated and compared. The elastic properties calculated both for η and η' are consistent with the available experimental results and other theoretical values, and explain the phenomenon happened in Al–Zn–Mg alloys well, which will be helpful for a comprehensive understanding of this material, providing assistance and guidance to the further study of such materials. Further experiments are needed to carried out to verify the

calculated elastic constants, especially for the metastable phase η'.

FUNDING

The work is financially supported by the National Natural Science Foundation of China (nos. U1637601, U1837207). Special thanks for the helpful discussions with Dolya Shieh and senior scientist Alf Zhu from University of Virginia!

REFERENCES

1. L. Shengdan, L. Chengbo, H. Suqi, D. Yunlai, and Z. Xinming, "Effect of natural aging on quench-induced inhomogeneity of microstructure and hardness in high strength 7055 aluminum alloy," J. Alloys Compd. **625**, 34–43 (2015).
2. F. Xigang, J. Daming, M. Qingchang, and Z. Li, "The microstructural evolution of an Al–Zn–Mg–Cu alloy during homogenization," Mater. Lett. **60**, 1475–1479 (2006).
3. Z. W. Du, Z. M. Sun, B. L. Shao, T. T. Zhou, and C. Q. Chen, "Quantitative evaluation of precipitates in an Al–Zn–Mg–Cu alloy after isothermal aging," Mater. Charact. **56**, 121–128 (2006).
4. X. M. Li and M. J. Starink, "Effect of compositional variations on characteristics of coarse intermetallic particles in overaged 7000 aluminium alloys," Mater. Sci. Technol. **17**, 1324–1328 (2001).
5. L. Guofeng, Z. Xinming, L. Penghui, and Y. Jianghai, "Effects of retrogression heating rate on microstructures and mechanical properties of aluminum alloy 7050," Trans. Nonferrous Met. Soc. China **20**, 935–941 (2010).
6. C. Songyi, C. Kanghua, P. Guosheng, J. Le, and D. Pengxuan, "Effect of heat treatment on strength, exfoliation corrosion and electrochemical behavior of 7085 aluminum alloy," Mater. Des. **35**, 93–98 (2012).
7. C. Wolverton, "Crystal structure and stability of complex precipitate phases in Al–Cu–Mg–(Si) and Al–Zn–Mg alloys," Acta Mater. **49**, 3129–3142 (2001).
8. J. Gjønnes and C. J. Simensen, "An electron microscope investigation of the microstructure in an aluminium–zinc–magnesium alloy," Acta Metall. **18**, 881–890 (1970).
9. J. H. Auld and S. M. Cousland, "On the structure of the M' phase in Al–Zn–Mg alloys," J. Appl. Crystallogr. **18**, 47–48 (1985).
10. C. Régnier, J. Bouvaist, and J. P. Simon, "Etude cristallographique de la phase de transition M" dans Al–8%Zn–1%Mg," J. Appl. Crystallogr. **15**, 590–593 (1982).
11. C. Ravi and C. Wolverton, "First–principles study of crystal structure and stability of Al–Mg–Si–(Cu) precipitates," Acta Mater. **52**, 4213–4227 (2004).
12. X. Z. Li, V. Hansen, J. GjOnnes, and L. R. Wallenberg, "HREM study and structure modeling of the η' phase, the hardening precipitates in commercial Al–Zn–Mg alloys," Acta Mater. **47**, 2651–2659 (1999).
13. A. Kverneland, V. Hansen, R. Vincent, K. Gjønnes, and J. Gjønnes, "Structure analysis of embedded nano-sized particles by precession electron diffraction. η'-precipitate in an Al–Zn–Mg alloy as example," Ultramicroscopy **106**, 492–502 (2006).
14. J. Z. Liu, J. H. Chen, D. W. Yuan, C. L. Wu, J. Zhu, and Z. Y. Cheng, "Fine precipitation scenarios of AlZnMg(Cu) alloys revealed by advanced atomic-resolution electron microscopy study Part I: Structure determination of the precipitates in AlZnMg(Cu) alloy," Mater. Charact. **99**, 277–286 (2015).
15. J. Z. Liu, J. H. Chen, D. W. Yuan, C. L. Wu, J. Zhu, and Z. Y. Cheng, "Fine precipitation scenarios of AlZnMg(Cu) alloys revealed by advanced atomic-resolution electron microscopy study Part II: Fine precipitation scenarios in AlZnMg(Cu) alloys," Mater. Charact. **99**, 142–149 (2015).
16. J. Z. Liu, J. H. Chen, D. W. Yuan, C. L. Wu, J. Zhu, and Z. Y. Cheng, "Precipitation behaviour of Al–Zn–Mg–Cu alloy and diffraction analysis from η' precipitates in four variants," J. Alloys Compd. **610**, 623–629 (2014).
17. L. Helge Bovik, T. Gunnar, N. Solvi, and P. Philip, "Average crystal structure(s) of the embedded meta stable η'-phase in the Al–Mg–Zn system," Philos. Mag. **94**, 1719–1743 (2014).
18. A. L. Garcia-Garcia, I. Dominguez-Lopez, L. Lopez-Jimenez, and J. D. Barceinas-Sanchez Oscar, "Comparative quantification and statistical analysis of η' and η precipitates in aluminum alloy AA7075–T651 by TEM and AFM," Mater. Charact. **87**, 116–124 (2014).
19. M. CalinD, L. Williams, A. SigmundJ, and F. Jesper, "Atomic structure of hardening precipitates in an Al–Mg–Zn–Cu alloy determined by HAADF–STEM and first-principles calculations: relation to η-$MgZn_2$," J. Mater. Sci. **48**, 3638–3651 (2013).
20. A. Kverneland, V. Hansen, G. Thorkildsen, H. B. Larsen, P. Pattison, X. Z. Li, and J. Gjønnes, "Transformations and structures in the Al–Zn–Mg alloy system: A diffraction study using synchrotron radiation and electron precession," Mater. Sci. Eng., A **528**, 880–887 (2011).
21. T. Seidenkranz and E. Hegenbarth, "Single–crystal elastic constants of $MgZn_2$ in the temperature range from 4.2 to 300 K," Phys. Status Solidi A **33**, 205–210 (1976).
22. W. Mengmeng, W. Li, T. Biyu, P. Liming, and D. Wenjiang, "First-principles study of elastic and electronic properties of MgZn2 and ScZn2 phases in Mg–Sc–Zn alloy," J. Alloys Compd. **506**, 412–417 (2010).
23. C. Qiang, H. Zhiwei, Z. Zude, and S. Dayu, "First principles study on elastic properties, thermodynamics and electronic structural of AB2 type phases in magnesium alloy," Solid State Commun. **162**, 1–7 (2013).
24. T. Bi-Yu, W. Na, Y. Wei-Yang, Z. Xiao-Qin, and D. Wen-Jiang, "Theoretical investigation of typical fcc precipitates in Mg-based alloys," Acta Mater. **56**, 3353–3357 (2008).
25. D. Shin and C. Wolverton, "First-principles study of solute-vacancy binding in magnesium," Acta Mater. **58**, 531–540 (2010).
26. P. Hohenberg and W. Kohn, "Inhomogeneous electron gas," Phys. Rev. B **136**, 864–847 (1964).

27. D. Vanderbilt, "Soft self-consistent pseudopotentials in a generalized eigenvalue formalism," Phys. Rev. B **41**, 7892–7895 (1990).
28. D. M. Ceperley and B. J. Alder, "Ground state of the electron gas by a stochastic method," Phys. Rev. Lett. **45**, 566–569 (1980).
29. J. P. Perdew and A. Zunger, "Self-interaction correction to density–functional approximations for many-electron systems," Phys. Rev. B **23**, 5048–5079 (1981).
30. J. P. Perdew, K. Burke, and M. Ernzerhof, "Generalized gradient approximation made simple," Phys. Rev. Lett. **77**, 3865–3868 (1996).
31. J. H. Westbrook, *Basic Mechanical Properties and Lattice Defects of Intermetallic Compounds*, Ed. by R. L. Fleischer (Wiley, 2000).
32. O. Yifang, L. Fenglian, C. Hongmei, T. Xiaoma, D. Yong, and H. Yuehui, "The structural stability, elastic constants and electronic structure of Al–Sr intermetallics by first-principles calculations," Phys. B **406**, 3681–3686 (2011).
33. Y. Han and J. Jung, "Structure and stability of Al13I clusters," J. Chem. Phys. **121**, 8500–8502 (2004).
34. N. A. Zarkevich, T. L. Tan, and D. D. Johnson, "First-principles prediction of phase-segregating alloy phase diagrams and a rapid design estimate of their transition temperatures," Phys. Rev. B **75**, 104203 (2007).
35. X. M. Li and M. J. Starink, "Identification and analysis of intermetallic phases in overaged Zr-containing and Cr–containing Al–Zn–Mg–Cu alloys," J. Alloys Compd. **509**, 471–476 (2011).
36. Z. Wu, E. Zhao, H. Xiang, X. Hao, X. Liu, and J. Meng, "Crystal structures and elastic properties of superhard IrN2 and IrN3 from first principles," Phys. Rev. B **76**, 054115 (2007).
37. R. Hill, "The elastic behaviour of a crystalline aggregate," Proc. Phys. Soc. Sect. A **65**, 349–354 (1952).
38. S. F. Pugh, "Relations between the elastic moduli and the plastic properties of polycrystalline pure metals," Philos. Mag. **45**, 823–843 (1954).
39. R. Hill, "On discontinuous plastic states, with special reference to localized necking in thin sheets," J. Mech. Phys. Solids **1**, 19–30 (1952).
40. M. Mattesini, R. Ahuja, and B. Johansson, "Cubic Hf3N4 and Zr3N4: A class of hard materials," Phys. Rev. B **68**, 184108 (2003).
41. V. Tvergaard and J.W. Hutchinson, "Microcracking in ceramics induced by thermal expansion or elastic anisotropy," J. Am. Ceram. Soc. **71**, 157–166 (2005).
42. W. Guo, J. Guo, J. Wang, M. Yang, H. Li, X. Wen, and J. Zhang, "Evolution of precipitate microstructure during stress aging of an Al–Zn–Mg–Cu alloy," Mater. Sci. Eng., A **634**, 167–175 (2015).